Journal of Cerebral Blood Flow & Metabolism (2007) 27, 839–849

www.jcbfm.com

When perfusion meets diffusion: *in vivo* measurement of water permeability in human brain

Jiongjiong Wang[1,2], María A Fernández-Seara[2], Sumei Wang[1] and Keith S St Lawrence[3]

[1]*Departments of Radiology, University of Pennsylvania, Philadelphia, Pennsylvania, USA;* [2]*Department of Neurology, University of Pennsylvania, Philadelphia, Pennsylvania, USA;* [3]*Lawson Health Research Institute, London, Ontario, Canada*

Quantification of water permeability can improve the accuracy of perfusion measurements obtained with arterial spin labeling (ASL) methods, and may provide clinically relevant information regarding the functional status of the microvasculature. The amount of labeled water in the vascular and tissue compartments in an ASL experiment can be estimated based on their distinct diffusion characteristics, and in turn, water permeability determined from the relative vascular and tissue contributions. In the present study, a hybrid magnetic resonance imaging technique was introduced by marrying a continuous ASL method with a twice-refocused spin–echo diffusion sequence. Series of diffusion-weighted ASL signals were acquired with systematically varied *b* values. The signals were modeled with fast and slow decaying components that were associated with the vascular and tissue compartments, respectively. The relative amount of labeled water in the tissue compartment increased from 61% to 74% and to 86% when the postlabeling delay time was increased from 0.8 to 1.2 and to 1.5 secs. With a *b* value of 50 secs/mm^2, the capillary contribution (fast component) of the ASL signal could be effectively minimized. Using the single-pass approximation model, the water permeability of gray matter in the human brain was estimated based on the derived relative water fractions in the tissue and microvasculature. The potential for *in vivo* magnetic resonance mapping of water permeability was showed using two diffusion weighted ASL measurements with *b* = 0 and 50 secs/mm^2 in both healthy subjects and a case of brain tumor.
Journal of Cerebral Blood Flow & Metabolism (2007) **27,** 839–849. doi:10.1038/sj.jcbfm.9600398; published online 13 September 2006

Keywords: arterial transit time; arterial spin labeling; water exchange rate; water permeability

Introduction

Arterial spin labeling (ASL) methods use magnetically labeled blood water as an endogenous contrast agent to measure perfusion (Detre and Wang, 2002). Although water was initially considered a freely diffusible tracer, cumulating evidence from nuclear medicine and magnetic resonance imaging studies have showed that there is limited exchange of water between the vascular (capillary) and tissue space (Ewing *et al*, 2001; Li *et al*, 2005; Parkes and Tofts, 2002; Silva *et al*, 1997*a, b*; St Lawrence *et al*, 2000; Zhou *et al*, 2001). Particularly, water permeability is an order of magnitude lower in the central nervous system than the systemic circulation, because the structure of the blood–brain barrier (BBB) only allows water molecules to be transported into brain tissue through the plasma membrane of endothelial cells instead of through cellular gaps (Paulson, 2002). With ASL methods, it is generally reasonable to ignore the effects of limited water exchange in the quantification of perfusion, provided that the relaxation rates in tissue and blood are similar (Parkes and Tofts, 2002; St Lawrence *et al*, 2000; St Lawrence and Wang, 2005). Nevertheless, analyzing ASL data with tracer kinetic models that include both tissue and vascular contributions may improve quantification in tissues, such as white matter, that have significantly different relaxation rates from blood (Li *et al*, 2005; Parkes and Tofts, 2002; St Lawrence *et al*, 2000; St Lawrence and Wang, 2005). These models also offer the opportunity to estimate water permeability, which could provide a surrogate index of the integrity of BBB and may reflect the status of microcirculation (Barbier *et al*, 2002). For instance, permeability of the BBB has been reported to vary with age and may be altered in neurodegenerative

Correspondence: Dr J Wang, Department of Radiology, Center for Functional Neuroimaging, University of Pennsylvania, 3 W Gates, 3400 Spruce Street, Philadelphia, Pennsylvania 19104, USA.
E-mail: wangj3@mail.med.upenn.edu
This research was supported by NIH Grants NS045839 and P41-RR02305.
Received 30 May 2006; revised 17 July 2006; accepted 1 August 2006; published online 13 September 2006

diseases, neoplasm, and during central nervous system infections (Larsson and Tofts, 1992; Law *et al*, 2004; Li *et al*, 2005; Roberts *et al*, 2000; Tofts and Kermode, 1991; Wolf *et al*, 2005). Estimation of water permeability, therefore, is important for improved perfusion quantification using ASL, as well as for assessing the functional status of the BBB.

Existing knowledge on water permeability came from studies that either directly measured the extraction fraction of labeled water (Friis *et al*, 1980; Paulson *et al*, 1977), or indirectly by comparison to perfusion values obtained with other tracers (Eichling *et al*, 1974; St Lawrence and Lee, 1998). Based on these results, several recent studies explored the effect of limited water permeability on perfusion quantification with ASL (Ewing *et al*, 2001; Li *et al*, 2005; Parkes and Tofts, 2002; St Lawrence *et al*, 2000; Zhou *et al*, 2001). A moderate, yet significant, perfusion error has been shown, which is generally larger in continuous than pulsed ASL methods, at high versus low magnetic field strength, in white matter compared with gray matter, and with high as opposed to low flow rates. Two studies included water permeability as a fitting parameter when analyzing ASL data acquired at multiple delay times (Li *et al*, 2005; Parkes and Tofts, 2002). However, the estimated water exchange rates from the two studies were considerably different and showed large intersubject variability. These differences could be attributed to the moderate sensitivity of the ASL signal to variations in water permeability because of the similarity of the relaxation rates in blood and brain tissue. In animal experiments, estimation of the water extraction fraction has been attempted with ASL by differentiating the fractions of labeled water in the vascular and tissue compartments (Silva *et al*, 1997*a, b*; Zaharchuk *et al*, 1998). This was achieved by suppressing the vascular signal using either diffusion gradients or a long-lived vascular contrast agent, or by suppressing the tissue signal through magnetization-transfer (MT) effects.

In the present study, we attempted to separate the vascular and tissue compartments in human brain with diffusion-weighted (DW) perfusion magnetic resonance imaging. A series of ASL perfusion scans with varying diffusion weightings were acquired to fit the fractions of ASL signals in the vascular and tissue compartments, which have fast and slow diffusion properties, respectively (Silva *et al*, 1997*a*). The single-pass approximation (SPA) model was used to determine the water exchange rate from the vascular and tissue fractions (St Lawrence *et al*, 2000; St Lawrence and Wang, 2005).

Methods

Imaging Sequence

The DW perfusion sequence was a hybrid of the amplitude-modulated continuous ASL (CASL) technique (Alsop and Detre, 1998; Wang *et al*, 2005*a*) and a twice-refocused spin–echo diffusion sequence supplied by the vendor (Reese *et al*, 2003) (Figure 1). Continuous ASL was performed with a 1.6 mT/m gradient and 2.25 μT RF irradiation applied 8 cm beneath the center of the acquired slices. An amplitude-modulated version of the labeling pulse based on a sinusoid function was used for control labeling with a modulation frequency of 100 Hz and peak amplitude of 3.18 μT. The tagging/control duration was 2.6 secs. Three delay times (0.8, 1.2, and 1.5 secs) between the end of the labeling pulse and image acquisition were used in the experiment. Interleaved images with and without labeling were acquired using a single-shot spin–echo echo-planar imaging (EPI) sequence with two refocusing pulses. Two pairs of bipolar gradients were applied along the slice direction (between the excitation pulse and EPI acquisition), with the RF refocusing pulses dividing each bipolar pair. Bipolar gradients with varying degrees of diffusion weighting were performed, namely $b = 0$, 25, 50, 100, 150, 200, and 300 secs/mm^2 for the delay time of 0.8 secs, and $b = 0$, 10, 25, 50, 100, and 200 secs/mm^2 for the delay times of 1.2 and 1.5 secs. We chose a lower maximum b value for the longer delay times because the perfusion signal relaxes with increasing delay. The durations of the four lobes of the bipolar gradients were optimized to minimize effects of eddy currents during EPI readout, and were 7, 11, 12, and 6 ms for the delay time of 0.8 sec, and 6, 10, 11, and 5 ms for the delay times of 1.2 and 1.5 secs, respectively. The maximum gradient strength was 31 mT/m with a ramp time of 200 μsecs.

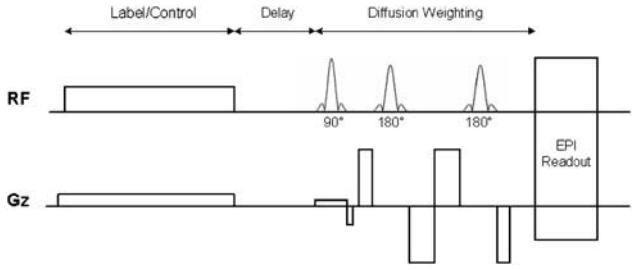

Figure 1 Diagram of the hybrid sequence combining CASL and twice-refocused spin–echo methods. RF and gradients along the slice direction are shown.

Magnetic Resonance Scanning

Magnetic resonance (MR) scanning was conducted on a Siemens 3.0 T Trio whole-body scanner (Siemens AG, Erlangen, Germany), using a standard Transmit/Receive (Tx/Rx) head coil. Written informed consent was obtained before all human studies according to a protocol approved by the University of Pennsylvania Institutional Review Board. Thirteen healthy subjects (6 women, aged 22 to 33 years, mean 26.4 years) participated in the experiment, with 5 subjects undergoing perfusion magnetic resonance imaging scanning with the 0.8 sec delay, 4 subjects scanned with the 1.2 secs delay, and the rest 4 subjects scanned with the 1.5 secs delay time. Acquisition

parameters were: FOV = 22 cm, matrix = 64 × 64, bandwidth = 3 kHz/pixel, 6/8 partial K-space, TR = 4.0 to 4.5 secs, TE = 60 (delay = 0.8 sec) or 55 ms (delay = 1.2 and 1.5 secs). Four slices (6 to 8 mm thickness with 2 to 3 mm gap) were acquired from inferior to superior in a sequential order, and each slice acquisition took approximately 90 ms. Each CASL scan with 80 acquisitions took 5.5 mins, which was repeated in each subject to acquire series of perfusion images with systematically varied b values (see above). The order of CASL scans with different diffusion weightings was counterbalanced across subjects.

Data Processing

The raw EPI images in each scan acquired at a particular b value and delay time were separated into label and control pairs and then pair-wise subtracted. Temporal fluctuations in the difference ASL image series owing to motion, physiologic noise, and residual eddy currents were minimized using an algorithm based on principal component analysis (Alsop and Detre, 1997), followed by averaging across the image series to form the mean ASL perfusion images (ΔM). The SPM software package was used to segment the raw EPI images into three whole brain regions of interest (ROI): gray matter, white matter, and cerebrospinal fluid. The mean ΔM signals were measured within the gray matter ROIs, which were fitted according to a bi-exponential model with the b value as the independent variable (Silva *et al*, 1997*a*):

$$\frac{\Delta M(b)}{\Delta M(0)} = A_1 \exp(-bD_1) + A_2 \exp(-bD_2) \qquad (1)$$

where the weighting factors, A_1 and A_2, are the fractions of the fast (vascular) and slow (tissue) components of the signal attenuation curve, respectively ($A_1 + A_2 = 1$), and D_1 and D_2 are the corresponding (pseudo-) apparent diffusion coefficients (ADCs). The fitting procedures were performed using the Origin 7.5 software package (OriginLab, Northampton, MA, USA) on each subject's data, as well as on the group ΔM signals averaged across all subjects for each delay time (0.8, 1.2, and 1.5 secs). The SPA model was used to interpret A_1 and A_2 in terms of water exchange between the vascular and tissue compartments (see the Appendix). Additionally, the raw EPI intensities of the control acquisitions (M) were measured within the gray matter ROIs, and fitted based on the bi-exponential model (equation (1)) as described above (Le Bihan and Turner, 1992). Note the ΔM signal represents the signal of the labeled water alone, whereas the M signal consists of static brain tissue and non-labeled water signals.

Single-Pass Approximation Model Simulation

To estimate water permeability from the fitted weighting factors A_1 and A_2, simulation was performed based on the SPA model including two compartments for capillary and brain tissue, using a program written in IDL (RSI, Boulder, CO, USA). Arterial and venous compartments were ignored owing to the use of a delay time in our experiment and minimal venous outflow within regular flow range (St Lawrence *et al*, 2000; St Lawrence and Wang, 2005). A numerical technique was used that divided a single capillary transit of the labeled spins (defined as the capillary volume, V_c, divided by the cerebral blood flow, f) into small, consecutive time segments ($n = 400$) to allow calculation of exchange effects in a stepwise fashion. Details of the theoretical background were described in our earlier publications (St Lawrence *et al*, 2000; St Lawrence and Wang, 2005). Assumed T1's for brain tissue (gray matter) and blood at 3.0 T were 1.26 and 1.49 secs (Wang *et al*, 2002), and T2's were 80, 120, and 40 ms for brain tissue (gray matter), arterial, and venous blood, respectively (St Lawrence and Wang, 2005). The arterial transit time (ATT) for the labeled spins to reach capillaries was assumed to be 1.4 secs based on our previous measurement (Wang *et al*, 2003). The ratio of extravascular (Se) and capillary (Sc) ASL signals was calculated whereas three parameters were systematically varied in the SPA model, that is, the permeability surface-area product (PS, from 20 to 400 in step of 20 ml/100 g min), V_c (from 0.4 to 3.0 in step of 0.2 ml/100 g) and f (from 30 to 105 in step of 15 ml/100 g min).

Patient Scanning

An improved hybrid technique, which combined a pseudo-CASL (pCASL) method (Garcia *et al*, 2005) with the twice-refocused spin–echo diffusion sequence, was used for clinical MR scanning on a brain tumor patient (21 years male, grade II oligodendroglioma), using the standard Tx/Rx head coil. Compared with the amplitude-modulated CASL, the pCASL approach provided improved labeling efficiency (~90%) and reduced MT effects (Fernandez-Seara *et al*, 2006). The pCASL pulse (Garcia *et al*, 2005) consisted of 1600 selective RF pulses, played sequentially, at equal spacing, for a 1.5-sec labeling duration. Each RF pulse was shaped as a modified Hanning window (peak/average $B_1 = 5.3/1.8\,\mu$T, duration = 500 μsecs, and peak/average $G = 6.0/2.3$ mT/m). Imaging parameters were: postlabeling delay time = 1.2 secs, TR/TE = 4500/46 ms, 22 cm FOV, 64 × 64 matrix, ten 8 mm slices with 2 mm gap. Two scans (80 acq each) with $b = 0$ and 50 secs/mm^2 were performed on the brain tumor patient. Data analyses followed the steps described above, and ROIs were manually drawn by a neuroradiologist (SW) in the solid part of the tumor, and normal gray matter on the same slices, based on structural MR images (FLAIR and T1 after contrast). Another ROI was also manually drawn in the tumor region manifesting high blood flow in the perfusion images acquired with $b = 0$ sec/mm^2. The mean difference ASL signals (ΔM) acquired with $b = 0$ and 50 secs/mm^2 were extracted in these three ROIs.

Results

Diffusion-Weighted Arterial Spin Labeling Signal Attenuation Curves

The bi-exponential fitting was successful in all subjects for the gray matter ΔM signals. Figure 2

shows attenuation curves of the mean ΔM and raw EPI (M) signals (within gray matter ROIs) with increasing b values acquired at the three delay times of 0.8 (A), 1.2 secs (B), and 1.5 secs (C). Figure 3 displays representative ΔM images with series of b values acquired at the three delay times. The ΔM signal curves appear to consist of a fast and a slow decaying component. The fast attenuation component becomes less obvious for the prolonged delay of 1.5 secs, as the labeled spins exchange into brain tissue with time. With the delay time of 0.8 secs, the fitted weighting factor for the slow component (A_2) was 61%, which increased to 74% and 86% when the delay time was prolonged to 1.2 and 1.5 secs, respectively. A relatively clean separation of the fast and slow components of the ΔM attenuation curve could be achieved with the b value of 50 secs/mm^2, at which there was only less than 2% signal of the fast decaying component, whereas the slow component still retained more than 95% of the signal.

Fitted parameters in each individual subject for the gray matter ROIs are listed in Tables 1, 2 and 3. In general, the bi-exponential model accounted well for the experimental data acquired with shorter delays of 0.8 and 1.2 secs, with a minimal correlation coefficient (R) of 0.90 between the estimated and experimental data. For the delay of 1.5 secs, the bi-exponential model accounted moderately well for the experimental data, with a minimal R of 0.68.

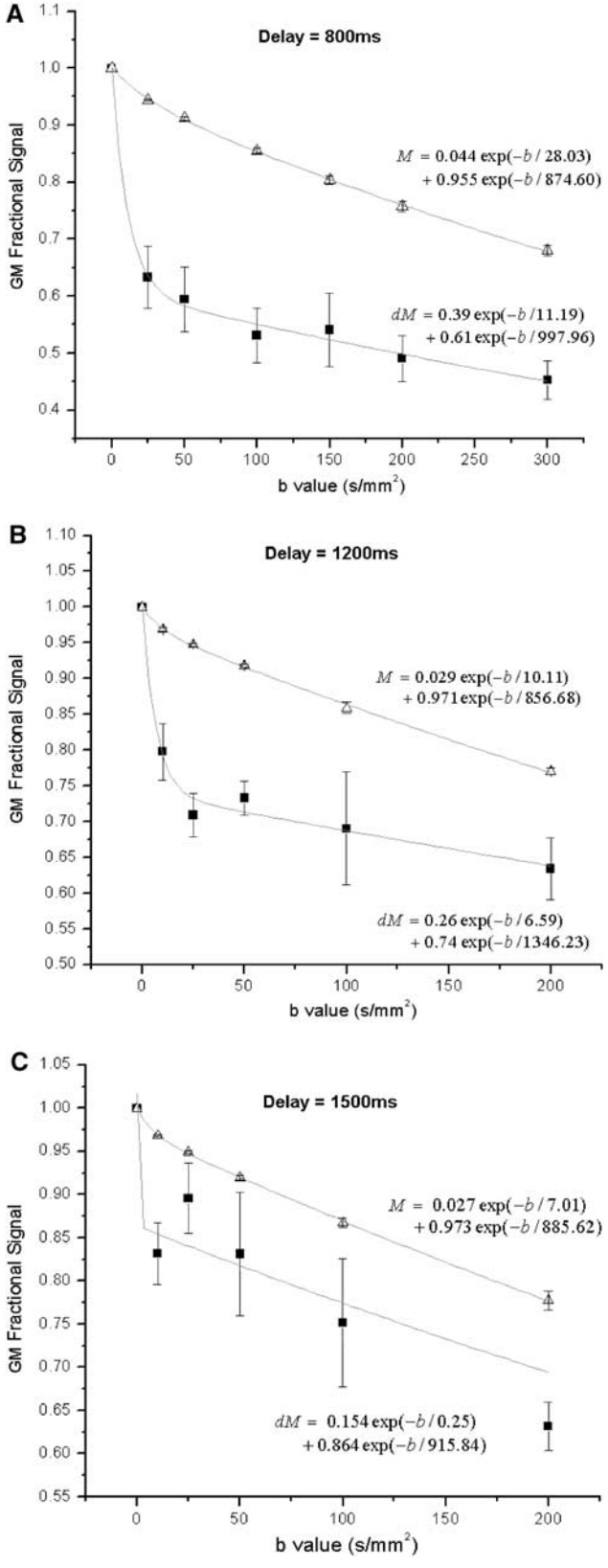

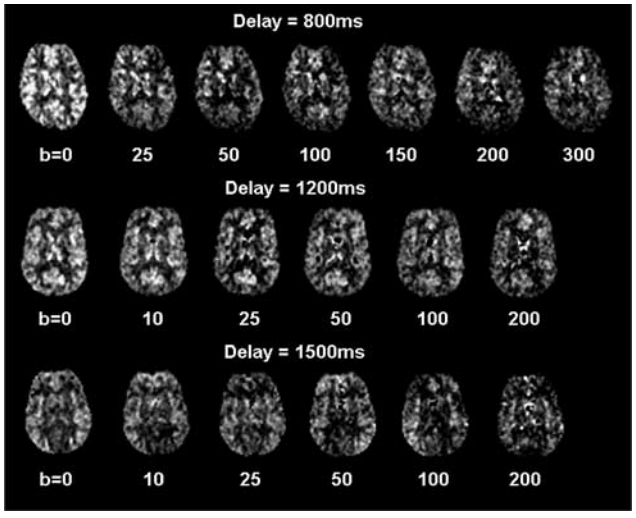

Figure 3 The ASL difference (ΔM) perfusion images of three representative subjects acquired with the delay time of 800, 1200, and 1500 ms, respectively. Series of ΔM images with varying diffusion weightings (b values) are shown. Reasonable image quality can be achieved with relatively large b values of 200 or 300 secs/mm^2.

Figure 2 The mean ASL signals (ΔM, filled square) and raw EPI intensities (M, open triangle) measured within the gray matter ROIs acquired with the delay time of 800 ms (**A**), 1200 ms (**B**), and 1500 ms (**C**). Data are normalized to the signals acquired without diffusion weighting ($b = 0$) in each subject, and averaged across subjects. Error bars indicate standard error. The bi-exponential decay model is fitted to the attenuation curves of the ΔM and M signal, and the results are shown as grey curves.

Table 1 Curve fitting results of the ΔM signals within gray matter ROI (acquired with the delay time of 0.8 secs) as a function of *b* value

Parameter	*Subject #1*	*Subject #2*	*Subject #3*	*Subject #4*	*Subject #5*	*Mean ± s.d.*	*Average curve*[a]
A_1	0.25	0.43	0.52	0.27	0.35	0.36 ± 0.11	0.39 ± 0.03
D_1^{-1} (s/mm^2)	10.26	0.03	3.20	0.65	0.21	2.87 ± 4.33	11.19 ± 2.91
A_2	0.75	0.57	0.48	0.73	0.65	0.64 ± 0.11	0.61 ± 0.02
D_2^{-1} (s/mm^2)	805	1137	906	512	893	851 ± 225	998 ± 192
R^2	0.99	0.89	0.97	0.89	0.95	0.94 ± 0.05	0.996

The analyses were performed in each individual subject and average ΔM signals across subjects. R is the correlation coefficient between measured and estimated ΔM signals.
[a]Results are shown as estimated parameter ± standard error, the 95% confidence interval equals estimated parameter ± 1.96 standard error.

Table 2 Curve fitting results of the ΔM signals within gray matter ROI (acquired with the delay time of 1.2 s) as a function of *b* value

Parameter	*Subject #1*	*Subject #2*	*Subject #3*	*Subject #4*	*Mean ± s.d.*	*Average curve*[a]
A_1	0.23	0.33	0.20	0.25	0.25 ± 0.06	0.26 ± 0.03
D_1^{-1} (s/mm^2)	4.04	9.68	0.25	9.64	5.90 ± 4.61	6.59 ± 2.24
A_2	0.77	0.67	0.79	0.76	0.75 ± 0.06	0.74 ± 0.02
D_2^{-1} (s/mm^2)	597	1089	2112	2781	1645 ± 985	1346 ± 483
R^2	0.995	0.91	0.82	0.80	0.88 ± 0.09	0.99
A_2/A	3.35	2.03	3.95	3.04	3.09 ± 0.80	2.85
PS/V_c (min^{-1})	209	126	246	190	193 ± 50	178

The analyses were performed in each individual subject and average ΔM signals across subjects. Also listed are estimated PS/V_c based on the SPA model.
[a]Results are shown as estimated parameter ± standard error, the 95% confidence interval equals estimated parameter ± 1.96 standard error.

Table 3 Curve fitting results of the ΔM signals within gray matter ROI (acquired with the delay time of 1.5 secs) as a function of *b* value

Parameter	*Subject #1*	*Subject #2*	*Subject #3*	*Subject #4*	*Mean ± SD*	*Average curve*[a]
A_1	0.17	0.17	0.17	0.15	0.17 ± 0.05	0.15 ± 0.09
D_1^{-1} (s/mm^2)	0.12	52.82	3.96	0.25	14.29 ± 14.87	0.25 ± 1.36
A_2	0.80	0.83	0.83	0.86	0.83 ± 0.06	0.86 ± 0.06
D_2^{-1} (s/mm^2)	829	553	960	915	814 ± 105	915 ± 549
R^2	0.82	0.76	0.93	0.46	0.74 ± 0.12	0.89

The analyses were performed in each individual subject and average ΔM signals across subjects.
[a]Results are shown as estimated parameter ± standard error, the 95% confidence interval equals estimated parameter ± 1.96 standard error.

Although the estimated ADCs (D_1 and D_2) showed relatively large intersubject variability and large confidence intervals of parameter estimation as listed in Tables 1–3, the fitted fractions (A_1 and A_2) of the fast and slow decaying components were quite stable. The difference in the estimated A_1 and A_2 values at the three delay times of 0.8, 1.2, and 1.5 secs reached statistical significance using analysis of variance ($F(2, 10) = 7.11$, $P = 0.011$). *Post hoc* analyses indicated that the difference in A_1 and A_2 was significant ($P < 0.05$, unpaired *t*-test, one-tail) between each pair of the delay times.

The raw EPI signal curves (M) could also be fitted with the bi-exponential decay model, with convergent results in every subject. The proportion of the fast decaying component ranged from 2% to 6%. As can be seen in Figure 2, the ADC of the slow decaying component of the M signal curve ($ADC^{-1} = 875$, 857, and 886 secs/mm^2 for 0.8, 1.2, and 1.5 secs delay, respectively) seemed higher than the counterparts of the ΔM signal curve ($ADC^{-1} = 998$, 1346, and 916 secs/mm^2 for 0.8, 1.2, and 1.5 secs delay, respectively). However, no statistically significant difference ($P > 0.1$) was detected by paired *t*-test (one-tail), suggesting that the slow decaying components of the ΔM and M signal curves may share common diffusion properties. This result suggests that the ADC values of the slow component of the ΔM and M signal may be interchangeable, thereby may improve the efficiency of parameter estimation to derive A_1 and A_2 from the ΔM signal curve.

Estimation of Water Permeability

Figure 4A shows the SPA model simulation results (ratio of extravascular and capillary signals, Se/Sc)

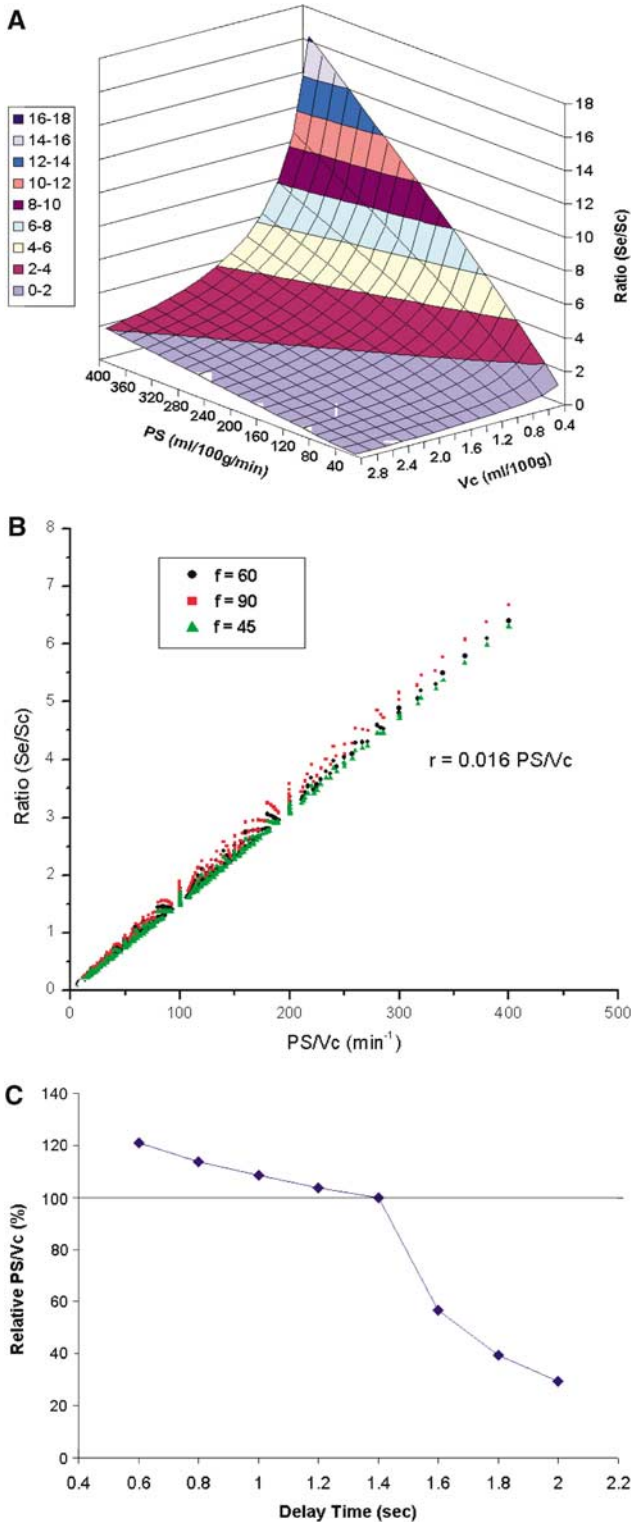

Figure 4 Simulation results based on the SPA model, showing (**A**) the ratio of Se/Sc as a function of PS and V_c ($f = 60$ ml/100 g min in this plot); (**B**) the ratio of Se/Sc as a function of PS/V_c at three different CBF levels; (**C**) the error in estimated PS/V_c as a function of delay time, assuming ATT = 1.4 secs and the delay time of 1.4 secs provides accurate estimation of PS/V_c. Note when delay time is greater than ATT, error in estimated PS/V_c quickly increases.

within wide ranges of V_c and PS ($f = 60$ ml/100 g min in this particular plot). Variations in V_c and PS exerted opposite effects on the ratio of Se and Sc. Although an increased PS facilitated the exchange of labeled spins into brain tissue (higher Se/Sc), a larger V_c retained more labeled spins in the vasculature (lower Se/Sc). As suggested by previous studies (Li *et al*, 2005; Parkes and Tofts, 2002; Zhou *et al*, 2001), the water exchange rate constant, defined as PS/V_c, is a critical parameter in the theoretical modeling of the water permeability effect (see Appendix). We therefore plotted the ratio of Se and Sc as a function of PS/V_c at various flow rates (Figure 4B), and a very good linear relationship (Se/Sc = 0.016 PS/V_c, $R = 0.998$, $P < 0.001$) was observed. It is worth noting that the above simulation result applies when the used delay time is equal to or slightly shorter than the ATT for the labeled spins to reach capillaries (assumed to be 1.4 secs). If the delay time is considerably shorter than ATT, there will be a significant arterial component in addition to the assumed capillary and tissue compartments in the SPA model. In contrast, if the delay time is longer than ATT, the capillary compartment will not be filled with labeled spins. Consequently, the relationship between Se/Sc and PS/V_c will be nonlinear (see Figure 4C). In our experiment, data acquired with the delay time of 1.2 secs generally satisfied the above presumption (especially considering each slice acquisition took approximately 90 ms). As listed in Table 2, the calculated mean PS/V_c was 193 ± 50 min^{-1} from four subjects.

From the acquired DW ASL data, it was possible to derive spatially resolved information of water permeability (exchange rate). In particular, a minimum of two-point ASL measurement with $b = 0$ and 50 secs/mm^2 could be used for this purpose (see Figure 2). As shown earlier, the diffusion gradient of $b = 50$ secs/mm^2 spoiled the majority of the fast component (vascular) signal (>98%), whereas retaining over 95% of the slow component (tissue) signal. The ΔM signal acquired at $b = 50$ secs/mm^2 can be treated as an approximation of the slow component signal, whereas the ΔM signal acquired at $b = 0$ represents the sum of the fast and slow component signals. The weighting factors A_1 and A_2 can therefore be directly estimated from the ratio of ΔM signals acquired at $b = 0$ and 50 secs/mm^2. Based on our experimental data acquired with the delay time of 1200 ms (Figure 2B), this simplified method with 2 ASL acquisitions ($b = 0$ and 50 secs/mm^2) may underestimate the PS/V_c by approximately 10% compared with multiple ASL measurements with b values up to 200 secs/mm^2. Representative images of PS/V_c from a single subject are displayed in Figure 5. To improve signal-to-noise ratio, a heavy spatial smoothing (full-width-at-half-maximum of two pixels) was applied to the ΔM images. In this particular subject, the mean PS/V_c in gray and white matter was 189 ± 56 and 166 ± 55 min^{-1}, respectively. This was expected because the ratio of the gray to white

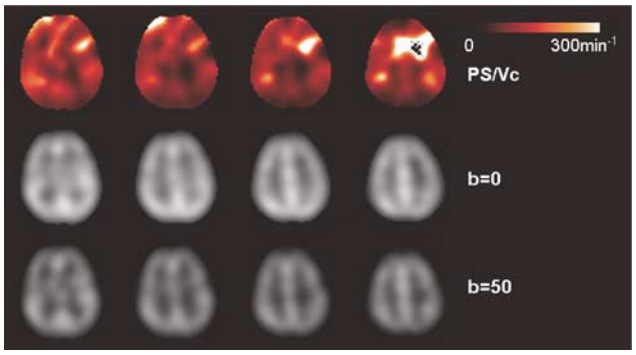

Figure 5 The ASL difference perfusion images of one representative subject acquired with $b = 0$ (middle row) and $b = 50\,\text{secs/mm}^2$ (bottom row) (delay time = 1200 ms), and the estimated PS/V_c images (top row). The ASL signals with $b = 50\,\text{secs/mm}^2$ are considered to only contain signals from brain tissue (slow decaying component), whereas the data with $b = 0$ represent the sum of vascular and tissue signals.

matter values for both the PS product and V_c are approximately the same (Herscovitch *et al*, 1987).

Clinical Application in Brain Tumor

The ASL images acquired with $b = 0$ and 50 secs/mm^2 of a 21-year-old male with grade II oligodendroglioma are displayed in Figure 6A, along with EPI and postcontrast T1-weighted (3D SPGR) structural images. The ASL images without DW showed focal hyperperfusion in the right frontal tumor region, which was largely preserved during the acquisition with $b = 50\text{secs/mm}^2$. In contrast, the perfusion signals in the surrounding gray matter were attenuated to a greater extent when the diffusion gradient of $b = 50\,\text{secs/mm}^2$ was applied. ROI analyses indicated that the fractional signal spoiled by the diffusion gradient was 16%, 20%, and 28% in the tumor region with high blood flow (blue), the solid part of tumor (red), and the normal gray matter (yellow), respectively (Figure 6). Based on SPA model simulation using the employed imaging parameters, and also assuming a constant ATT of 1.4 secs, the estimated PS/V_c was increased in the tumor region with high flow (generally corresponding to the aggressively growing part) (463.4 min^{-1}) as well as the solid part of tumor (347.8 min^{-1}) compared with the surrounding gray matter (223.6 min^{-1}). This result is consistent with the postcontrast T1 images showing a focal enhancement (moderate degree) within the posterior part of the lesion (arrow). Caution has to be exercised in interpreting increased PS/V_c observed in brain tumor as increased water permeability, given that potential changes in V_c and ATT may lead to similar observations. The confounding effects on quantification of water permeability in brain tumor will be discussed below.

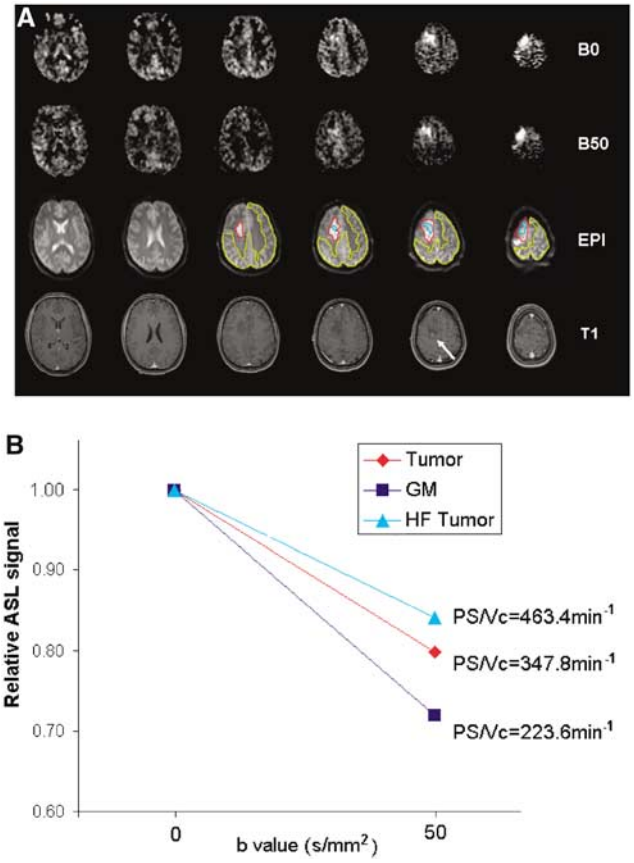

Figure 6 The ASL difference perfusion images of one brain tumor patient (21 year male, grade II oligodendroglioma) acquired with $b = 0$ and 50 secs/mm^2 (delay time = 1200 ms), along with raw EPI and post-contrast 3D T1 weighted SPGR structural images (**A**). Hand drawn ROIs of the tumor region with high blood flow (HF tumor), the solid part of tumor and the normal gray matter (GM) are shown in blue, red, and yellow, respectively. Signal enhancement in the postcontrast 3D T1-weighted SPGR images is indicated by an arrow. Mean relative ASL signal changes when b increases from 0 to 50 secs/mm^2 in the three ROIs are also shown (**B**).

Discussion

The present study showed a fast and a slow decaying component in the attenuation curves of ASL signals acquired with varying degrees of diffusion weighting (b value). The results are consistent with earlier animal studies (Silva *et al*, 1997*a, b*), supporting a limited exchange rate of blood water across the BBB. However, in the previous animal study (Silva *et al*, 1997*a*), MR signal acquisition was performed immediately after the labeling pulses, leaving the possibility that the observed fast decay may arise primarily from large arteries. In the present study, a delay time was used between labeling pulses and image acquisition to minimize the effect of arterial contributions in the

ASL signal (Alsop and Detre, 1996). The fast decay we observed should be attributed primarily to labeled spins in arterioles and capillaries. With a prolonged delay time, the observed tissue fraction of labeled water (A_2) was significantly increased compared with that measured at a shorter delay time, suggesting that the labeled spins gradually exchange into brain tissue with time. Nevertheless, even with a relatively long delay time of 1.5 secs, the tissue fraction was still significantly lower than 100% ($P<0.001$, unpaired *t*-test, one-tail), providing further evidence for the limited exchange of blood water (St Lawrence *et al*, 2000).

The limited exchange of blood water detected using our method is consistent with previous physiologic findings (Paulson, 2002; Paulson *et al*, 1977). Specifically, two related physical/physiologic processes contribute to the permeability of capillary wall to water molecules: water diffusion (i.e., the passage of water across the capillary wall in consequence of Brownian movements) and water filtration (i.e., the movement of water across the capillary wall in presence of an osmotic or hydrostatic pressure gradient). In capillaries outside the central nervous system, slits and pores between endothelial cells have major influence on water filtration because bulk flow across the capillary wall can take place through these pores and slits. However, pores or slits between the endothelial cells will only have minor influence of water diffusion because the total surface area of these pores and slits is a very small part of the whole capillary surface area. Within the central nervous system, however, aquaporins only allow for water diffusion and not for water filtration because the diameter of aquaporins is on the order of a single water molecule. Therefore, the ratio between water filtration and diffusion across the BBB is close to unity whereas it is fifty or more outside the central nervous system (e.g., muscles).

In the present study, the definitions of the weighting factors A_1 and A_2 in the bi-exponential model primarily depend on the water exchange rate constant PS/V_c as well as the tissue relaxation rate R_1 (see equation (A.4) in Appendix). This is in contrast to previous studies that interpreted these weighting factors in terms of the water extraction fraction (E); that is, $A_1=1-E$ and $A_2=E$ (Silva *et al*, 1997*a, b*; Zaharchuk *et al*, 1998). Their interpretation was based on the assumption that the extraction of labeled water into the tissue is instantaneous and consequently, relaxation of the label in the capillary bed is ignored. However, exchange occurs throughout the passage of water from the arterial to venous side of the capillary bed. Considering that the mean capillary transit time (i.e., V_c/f) is similar in value to T_1, both water exchange and relaxation should be accounted for when defining the concentrations of labeled water in the tissue and capillary compartments. Another reason we avoid the use of water extraction fraction is that it depends on several imaging parameters such as the duration of labeling pulses and postlabeling delay time.

One challenge for estimating water permeability using the DW ASL method is to reliably and accurately measure ASL signals in the presence of large diffusion gradients, which spoil a considerable portion of ASL signals. The somewhat inevitable eddy currents magnify the temporal fluctuations of the raw images, thereby affecting the accuracy of perfusion measurements relying on signal averaging across image series. On top of these effects, the signal-to-noise ratio in ASL methods is inherently low. These factors combined probably explain why there has been only one MR study in animals using the DW ASL approach and only FID signals (not imaging data) were recorded during that experiment (Silva *et al*, 1997*a*). In the present study, we were able to acquire ASL images with b values up to 300 secs/mm^2. This was building on two recent technical advancements including improved signal-to-noise ratio through implementation of ASL at high magnetic field (Wang *et al*, 2002; Wang *et al*, 2005*a*), and minimized effects of eddy currents using the twice-refocused spin–echo diffusion sequence (Reese *et al*, 2003). The temporal fluctuation level of the raw EPI images acquired with large diffusion gradients ($b=200$ or 300 secs/mm^2) was about twice that acquired with no diffusion weighting ($b=0$). A principal component analysis-based algorithm was used to reduce effects of temporal instability of raw EPI image series on perfusion images (Alsop and Detre, 1997). We were able to reliably measure DW ASL signals at least in large ROIs with relatively high blood flow (e.g., gray matter) in the present study. The image quality of the proposed technique was further improved through implementation of novel spin labeling schemes with improved efficiency (Garcia *et al*, 2005), as shown in the case of brain tumor. Additionally, the use of array coil for image acquisition in ASL perfusion magnetic resonance imaging has been shown to provide more than two-fold signal gain compared with a standard transmit/receive coil (Wang *et al*, 2005*b*). Temporal stability of the DW image series may be further improved with background suppression techniques (St Lawrence *et al*, 2005; Ye *et al*, 2000).

The methodological scheme of the proposed DW ASL method is analogous to the FEAST (Wang *et al*, 2003) and other ASL techniques using flow-spoiling gradients (Ye *et al*, 1997). However, given the main goal was to spoil intravascular signals, the majority of existing ASL methods used bipolar gradients with relatively weak strength (maximum $b=10$ to 20 secs/mm^2). Additionally, these studies used a short or even no postlabeling delay time so that the effect of intravascular signals was visible. In the present study, a relatively long delay time was applied to allow the majority of labeled spins to reach microvasculature, along with strong diffusion gradients to separate ASL signals in the capillary and tissue

compartments. Depending on the choice of these two parameters, that is, delay time and diffusion gradient strength, ASL techniques can be made to be primarily sensitive to signals from one of the arterial, capillary, and tissue compartments. The intrinsic diffusion weighting of the EPI readout echo train has been estimated to be on the order of 10^{-4} secs/mm^2, therefore was ignored in our experiment.

Our estimation of water permeability ($PS/V_c = 193 \pm 50\ min^{-1}$) of human brain is in line with literature values in a number of species. It has been reported that capillary space contains approximately 33% of the total blood volume (Sharan *et al*, 1989; van Zijl *et al*, 1998). Assuming a total blood volume of 4.5 ml/100 g in the gray matter (Zhou *et al*, 2001), V_c is on the order of 1.5 ml/100 g, which leads to a PS value of approximately 280 ml/100 g min in our study. Reported PS values in the cortex ranged from 50 to over 170 ml/100 g min in mammals including rat (54 ml/100 g min, Bolwig and Lassen, 1975), monkey (114 ml/100 g min, Eichling *et al*, 1974; 173 ml/100 g min, Larson *et al*, 1987), baboon (104 ml/100 g min, Raichle *et al*, 1983), and human (144 ml/100 g min, Paulson *et al*, 1977; 104 ml/100 g min, Herscovitch *et al*, 1987). Our estimation of PS is above the reported range, which may be affected by the choices of V_c, delay time and ATT. Nevertheless, the intersubject variability of the estimated water exchange rate and permeability is considerably smaller than other MR-based approaches (Li *et al*, 2005; Parkes and Tofts, 2002).

Using an improved DW ASL technique, the brain tumor case showed increased water permeability in either tumor region with high flow or the solid part of tumor, as compared with surrounding gray matter. This result was consistent with postcontrast T1-weighted images showing a moderate degree of signal enhancement. However, the accuracy of PS/V_c quantification may be confounded by potential variations in ATT between tumor and normal tissue, as shown in the simulation results of Figure 4C. Ideally, the FEAST technique needs to be performed for estimation of ATT in brain tumor. Limited by time, this was not possible in our clinical scan. Nevertheless, we showed that DW ASL images ($b = 50$ secs/mm^2) with reasonable quality can be obtained in a clinical setting, which have the potential for quantitative mapping of water permeability. Alternatively, to minimize the effect of variable ATT, we may perform DW ASL scans at a shorter delay time ($\leq$ ATT, e.g., 0.8 secs) with a small b value (e.g., 8 secs/mm^2) to spoil the arterial signals. Such scan represents the summation of capillary and tissue signals, which, in conjunction with the $b = 50$ secs/mm^2 scan, can be used for accurate estimation of PS/V_c. This direction is actively being pursued in our lab.

One caveat of the present study is that we assume the fast and slow components correspond to the capillary and tissue compartments for estimation of PS/V_c (with the delay time of 1.2 secs). It is possible that the fast component may contain residual arterial and arteriolar contributions, and that the slow component may contain contributions from capillaries and venules as well. This issue certainly merits further investigation. Another caveat of the present study is the MT effect caused by the long labeling pulses, which may reduce the tissue ASL signal through shortened T1. We assessed the magnitude of the MT effect following the approach proposed by Ye *et al*. (1997). In the presence of continuous labeling pulses, the T1 of brain tissue reduced from approximately 1.3 to 0.9 secs. However, the majority of tissue ASL signals recovered during the long delay of 1.2 secs, resulting in only 3% reduction in measured ASL signal as indicated by simulation using the SPA model. In the case of pseudo-continuous labeling pulses, the MT-induced signal reduction was even smaller. The MT effect was therefore ignored in our model to estimate water permeability. In the present study, diffusion gradients were applied along the slice direction. Because blood flow in the microvasculature and tissue (perfusion) is generally considered without a preferential direction (i.e., isotropic) (Mchedlishvili, 1986), we expect to replicate the attenuation curves of the ΔM signal when diffusion gradients are applied along the x and y-axis or any other direction. Nevertheless, a potential benefit for applying diffusion gradients simultaneously along two or three directions is a shortened TE, which may lead to improved signal-to-noise ratio.

Conclusion

By marrying diffusion and perfusion magnetic resonance imaging, we were able to differentiate the signal contributions from capillaries and brain tissue in an ASL experiment, which could potentially be used to estimate water permeability of human brain.

Acknowledgements

The authors are grateful to Dr John Detre for his helpful comments, Dr Ronald Wolf for his help with the clinical scan.

References

Alsop DC, Detre JA (1996) Reduced transit-time sensitivity in noninvasive magnetic resonance imaging of human cerebral blood flow. *J Cereb Blood Flow Metab* 16:1236–49

Alsop DC, Detre JA (1997) Reduction of excess noise in fMRI time series data using noise image templates (abstr). *Proc Int Magn Reson Med* 5:1687

Alsop DC, Detre JA (1998) Multisection cerebral blood flow MR imaging with continuous arterial spin labeling. *Radiology* 208:410–6

Barbier EL, St Lawrence KS, Grillon E, Koretsky AP, Decorps M (2002) A model of blood–brain barrier permeability to water: accounting for blood inflow and longitudinal relaxation effects. *Magn Reson Med* 47:1100–9

Bolwig TG, Lassen NA (1975) The diffusion permeability to water of the rat blood–brain barrier. *Acta Anesth Scand* 93:415–22

Detre JA, Wang J (2002) Technical aspects and utilities of fMRI using BOLD and ASL. *Clin Neurophysiol* 113:621–34

Eichling JO, Raichle ME, Grubb Jr RL, Ter-Pogossian MM (1974) Evidence of the limitations of water as a freely diffusible tracer in brain of the rhesus monkey. *Circ Res* 35:358–64

Ewing JR, Cao Y, Fenstermacher J (2001) Single-coil arterial spin-tagging for estimating cerebral blood flow as viewed from the capillary: relative contributions of intra- and extravascular signal. *Magn Reson Med* 46:465–75

Fernandez-Seara MA, Wang Z, Wang J, Korczykowski M, Guenther M, Feinberg DA, Detre JA (2006) 3 T pseudo-continuous ASL perfusion fMRI with background-suppressed single shot 3D GRASE during memory encoding. *Proc Int Soc Magn Reson Med* 14:378

Friis ML, Paulson OB, Hertz MM (1980) Carbon dioxide permeability of the blood–brain barrier in man. The effect of acetazolamide. *Microvasc Res* 20:71–80

Garcia DM, de Bazelaire C, Alsop D (2005) Pseudo-continuous flow driven adiabatic inversion for arterial spin labeling. *Proc Int Soc Magn Reson Med* 13:37

Herscovitch P, Raichle ME, Kilbourn MR, Welch MJ (1987) Positron emission tomographic measurement of cerebral blood flow and permeability-surface area product of water using [15O]water and [11C]butanol. *J Cereb Blood Flow Metab* 7:527–42

Larson KB, Markham J, Raichle ME (1987) Tracer-kinetic models for measuring cerebral blood flow using externally detected radiotracers. *J Cereb Blood Flow Metab* 7:443–63

Larsson HB, Tofts PS (1992) Measurement of blood–brain barrier permeability using dynamic Gd-DTPA scanning—a comparison of methods. *Magn Reson Med* 24:174–6

Law M, Yang S, Babb JS, Knopp EA, Golfinos JG, Zagzag D, Johnson G (2004) Comparison of cerebral blood volume and vascular permeability from dynamic susceptibility contrast-enhanced perfusion MR imaging with glioma grade. *AJNR Am J Neuroradiol* 25:746–55

Le Bihan D, Turner R (1992) The capillary network: a link between IVIM and classical perfusion. *Magn Reson Med* 27:171–8

Li KL, Zhu X, Hylton N, Jahng GH, Weiner MW, Schuff N (2005) Four-phase single-capillary stepwise model for kinetics in arterial spin labeling MRI. *Magn Reson Med* 53:511–8

Mchedlishvili G (1986) *Arterial behavior and blood circulation in the brain*. New York: Plenum Press

Parkes LM, Tofts PS (2002) Improved accuracy of human cerebral blood perfusion measurements using arterial spin labeling: accounting for capillary water permeability. *Magn Reson Med* 48:27–41

Paulson OB (2002) Blood–brain barrier, brain metabolism and cerebral blood flow. *Eur Neuropsychopharmacol* 12:495–501

Paulson OB, Hertz MM, Bolwig TG, Lassen NA (1977) Filtration and diffusion of water across the blood–brain barrier in man. *Microvasc Res* 13:113–24

Raichle ME, Martin WR, Herscovitch P, Mintun MA, Markham J (1983) Brain blood flow measured with intravenous H2(15)O. II. Implementation and validation. *J Nucl Med* 24:790–8

Reese TG, Heid O, Weisskoff RM, Wedeen VJ (2003) Reduction of eddy-current-induced distortion in diffusion MRI using a twice-refocused spin echo. *Magn Reson Med* 49:177–82

Roberts HC, Roberts TP, Brasch RC, Dillon WP (2000) Quantitative measurement of microvascular permeability in human brain tumors achieved using dynamic contrast-enhanced MR imaging: correlation with histologic grade. *AJNR Am J Neuroradiol* 21:891–9

Sharan M, Jones Jr MD, Koehler RC, Traystman RJ, Popel AS (1989) A compartmental model for oxygen transport in brain microcirculation. *Ann Biomed Eng* 17:13–38

Silva AC, Williams DS, Koretsky AP (1997*a*) Evidence for the exchange of arterial spin-labeled water with tissue water in rat brain from diffusion-sensitized measurements of perfusion. *Magn Reson Med* 38:232–7

Silva AC, Zhang W, Williams DS, Koretsky AP (1997*b*) Estimation of water extraction fractions in rat brain using magnetic resonance measurement of perfusion with arterial spin labeling. *Magn Reson Med* 37:58–68

St Lawrence KS, Lee TY (1998) An adiabatic approximation to the tissue homogeneity model for water exchange in the brain: II. Experimental validation. *J Cereb Blood Flow Metab* 18:1378–85

St Lawrence KS, Wang J (2005) Effects of the apparent transverse relaxation time on cerebral blood flow measurements obtained by arterial spin labeling. *Magn Reson Med* 53:425–33

St Lawrence KS, Frank JA, McLaughlin AC (2000) Effect of restricted water exchange on cerebral blood flow values calculated with arterial spin tagging: a theoretical investigation. *Magn Reson Med* 44:440–9

St Lawrence KS, Frank JA, Bandettini PA, Ye FQ (2005) Noise reduction in multi-slice arterial spin tagging imaging. *Magn Reson Med* 53:735–8

Tofts PS, Kermode AG (1991) Measurement of the blood–brain barrier permeability and leakage space using dynamic MR imaging. 1. Fundamental concepts. *Magn Reson Med* 17:357–67

van Zijl PC, Eleff SM, Ulatowski JA, Oja JM, Ulug AM, Traystman RJ, Kauppinen RA (1998) Quantitative assessment of blood flow, blood volume and blood oxygenation effects in functional magnetic resonance imaging. *Nat Med* 4:159–67

Wang J, Alsop DC, Li L, Listerud J, Gonzalez-At JB, Schnall MD, Detre JA (2002) Comparison of quantitative perfusion imaging using arterial spin labeling at 1.5 and 4.0 Tesla. *Magn Reson Med* 48:242–54

Wang J, Alsop DC, Song HK, Maldjian JA, Tang K, Salvucci AE, Detre JA (2003) Arterial transit time imaging with flow encoding arterial spin tagging (FEAST). *Magn Reson Med* 50:599–607

Wang J, Zhang Y, Wolf RL, Roc AC, Alsop DC, Detre JA (2005*a*) Amplitude modulated continuous arterial spin labeling perfusion MR with single coil at 3T-feasibility study. *Radiology* 235:218–28

Wang Z, Wang J, Connick TJ, Wetmore GS, Detre JA (2005*b*) Continuous ASL perfusion MRI with an array coil and parallel imaging at 3 T. *Magn Rason Med* 54:732–7

Wolf RL, Wang J, Wang S, Melhem ER, O'Rourke DM, Judy KD, Detre JA (2005) Grading of CNS neoplasms using continuous arterial spin labeled perfusion MR. *J Magn Reson Imaging* 22:475–82

Ye FQ, Frank JA, Weinberger DR, McLaughlin AC (2000) Noise reduction in 3D perfusion imaging by attenuating the static signal in arterial spin tagging (ASSIST). *Magn Reson Med* 44:92–100

Ye FQ, Mattay VS, Jezzard P, Frank JA, Weinberger DR, McLaughlin AC (1997) Correction for vascular artifacts in cerebral blood flow values measured by using arterial spin tagging techniques. *Magn Reson Med* 37:226–35

Zaharchuk G, Bogdanov Jr AA, Marota JJ, Shimizu-Sasamata M, Weisskoff RM, Kwong KK, Jenkins BG, Weissleder R, Rosen BR (1998) Continuous assessment of perfusion by tagging including volume and water extraction (CAPTIVE): a steady-state contrast agent technique for measuring blood flow, relative blood volume fraction, and the water extraction fraction. *Magn Reson Med* 40:666–78

Zhou J, Wilson DA, Ulatowski JA, Traystman RJ, van Zijl PC (2001) Two-compartment exchange model for perfusion quantification using arterial spin tagging. *J Cereb Blood Flow Metab* 21:440–55

Appendix

The amount of labeled water in the tissue volume as defined by the SPA model, $\Delta M_{SPA}(t)$, can be separated into two compartments:

$$\Delta M_{SPA}(t) = \Delta M^{c}_{SPA}(t) + \Delta M^{b}_{SPA}(t), \qquad (A.1)$$

where $\Delta M^{c}_{SPA}(t)$ is the capillary contribution and $\Delta M^{b}_{SPA}(t)$ is the brain tissue contribution. Because we used a delayed-acquistion approach, arterial contributions were ignored. As well, the venous contribution was assumed negligible because of T_1 and T_2 relaxation of the labeled blood (St Lawrence and Wang, 2005). In terms of the SPA model, the weighting factors, A_1 and A_2, in equation (1) are defined as

$$A_1 = \frac{\Delta M^{c}_{SPA}(t)}{\Delta M_{SPA}(t)} \text{ and } A_2 = \frac{\Delta M^{b}_{SPA}(t)}{\Delta M_{SPA}(t)} \qquad (A.2)$$

For illustrative purposes, we present the definitions of $\Delta M^{c}_{SPA}(t)$ and $\Delta M^{b}_{SPA}(t)$ under the simplest labeling condition, that is, steady-state continuous labeling:

$$\begin{aligned} \Delta M^{c}_{SPA}(t \to \infty) &= \left(\tfrac{2M_0}{\lambda}\right)\left(\tfrac{E^* f}{PS/V_c + R_{1a}}\right), \\ \Delta M^{b}_{SPA}(t \to \infty) &= \left(\tfrac{2M_0}{\lambda}\right)\left(\tfrac{E^* f}{(PS/V_c + R_{1a})R_1}\right)\left(\tfrac{PS}{V_c}\right), \end{aligned} \qquad (A.3)$$

where f is cerebral blood flow, PS is the permeability surface-area product, V_c is the capillary distribution volume of water, $R_1 = 1/T_1$, $R_{1a} = 1/(T_1$ of arterial blood), $E^* = 1 - e^{-PS/f - R_{1a}\tau_c}$, and τ_c is the capillary transit time $(= V_c/f)$(St Lawrence *et al*, 2000). Inserting these definitions into equation (A.2), the weighting factors are

$$A_1 = \frac{R_1}{PS/V_c + R_1} \text{ and } A_2 = \frac{PS/V_c}{PS/V_c + R_1} \qquad (A.4)$$

Equation (A.4) shows the direct relationship between the weighting factors and the water exchange rate constant, PS/V_c, which defines the flux of labeled water from capillaries into tissue. As with previous studies (Li *et al*, 2005; Parkes and Tofts, 2002), it is not possible to obtain an estimate of the PS product alone because the total flux into the tissue is governed by both PS and V_c.

The simple definitions of A_1 and A_2 presented in equation (A.4) ignore vacular transit times, the labeling duration, the acquisition delay, T_2 weighting and magnetization transfer effects. To determine the exchange rate constant, PS/V_c, from the experimentally determined weighting factors A_1 and A_2, general solutions for $\Delta M^{c}_{SPA}(t)$ and $\Delta M^{b}_{SPA}(t)$ that included all of these factors were used (St Lawrence and Wang, 2005). These solutions were solved numerically, as discussed in the Methods section, to determine the the best-fit value for PS/V_c from the experimental values of A_1 and A_2. This analysis was only conducted on the data collected with a delayed acquisition of 1.2 secs to avoid significant arterial contributions (Wang *et al*, 2003).